measured static and pitot pressures farther away from the oblique shock wave. The good correspondence between the predicted and measured pressure rise indicated, establishes confidence in the actual pressure change across the oblique shock wave and allows an appraisal of the region of probe influence. The increase in pitot pressure across the oblique shock wave is also compatible with that calculated using the oblique shock relations, e.g., experimentally $p_{t_2}'/p_{t_1}' = 1.48$, while a value of 1.50 is predicted. Of note in this connection is that the turning of the flow through an angle of 8.3° in passing through the oblique shock wave apparently did not influence the pitot tube reading downstream where the flow is inclined to the probe. The slight "blip" in the pitot pressure below the oblique shock wave is associated with a small disturbance locally in the flow rather than the presence of the oblique shock wave. This view is supported by pitot measurements at axial distances farther upstream and downstream which indicated the disturbance to lie along a streamline and thus was located at different radial distances from the oblique shock wave.

Rather large deviations in Mach number are found by using the local static and pitot pressures measured to calculate the Mach number; this occurs because of the fallacious static pressure readings. It should be mentioned that the upstream Mach number of 3.48 is not compatible with the static to total pressure ratio $p/p_{t_0} = 0.0116$ for isentropic flow up to the shock wave because the actual stagnation pressure upstream of the wave is less than the upstream reservoir pressure $p_{t_0} =$ 100 psia that is used to normalize the data. The reduction in stagnation pressure resulted from the flow passing through another oblique shock wave farther upstream.

The influence of the size of the static pressure probe on its reading is shown in Fig. 2. These measurements were made 0.5 in. downstream of those shown in Fig. 1 at a location where the static pressure was lower. The small probe is similar to that used upstream, and the larger probe is twice as long. Confidence in the actual pressure changes across the oblique shock wave is provided by the very good check with the predicted oblique shock relation shown as a dashed curve and the coincidence of both probe readings farther away from the oblique shock wave. The probes are shown at various locations to assist in the discussion of the readings.

Upstream of the oblique shock wave (Fig. 2) the larger probe readings do not have as pronounced a "hump" as observed with the small probe. Also there is a more gradual approach to the actual static pressure which is found farther away from the oblique shock wave, although this change is small for a probe that is twice as long.

Downstream of the oblique shock wave (Fig. 2) the small probe behavior is similar to that observed before in Fig. 1, although the actual static pressure does not appear to be recovered until the tip of the probe is located downstream of the oblique shock wave (a distance of 0.13 in. above the wave). The larger probe reading at this location is also in general agreement with the actual pressure. However, farther away from the oblique shock wave in the vicinity where the tip of the larger probe intersects the wave, there is a depression in the static pressure reading. The static pressure is recovered again at about 0.3 in., similar to that observed with the smaller probe when its tip was located downstream of the oblique shock wave. Apparently, once the tip of the probe is downstream of the wave, useful static pressure readings are obtained; although for longer probes meaningful readings also are found when the tip is upstream of the wave and the hole therefore is isolated downstream. Probes extending a great distance upstream would display this latter behavior too. When the probe tip is located downstream of the wave, the flow along the probe in the vicinity of the hole has originated from a location that lies above the probe (Fig. 2, flow arrows) and therefore, is apparently not influenced much by the probe bow shock-oblique shock wave interaction, and the presence of the oblique shock wave.

Summary and Conclusions

For a relatively short static pressure probe traversed across an oblique shock wave, the readings upstream of the wave were influenced by interactions at a lateral distance up to about one probe length l from the wave (15-probe diameters); although for a probe twice as long and about twice the diameter of the small probe, this lateral distance was only slightly more than $\frac{1}{2}$ the probe length. Downstream of the oblique shock wave useful static pressures were obtained once the tip of the probe was downstream of the wave (a lateral distance of about $l \tan\beta$ where β is the wave angle); although for longer probes meaningful readings are also found where the tip is upstream of the wave and the hole is isolated downstream. These trends would be the same if the wave angle β were negative rather than positive, since the results would be a mirror image of those shown. Clearly there are limitations on the use of such static pressure probes in the vicinity of shock waves; for example, in interaction studies of shock wave impingement and reflection from boundary layers.

References

[1] Cronvich, L. L., "Pressure Distributions Over a Cylinder with Conical or Hemispherical Head at Supersonic Velocities," Rept. CM-528, Feb. 1949, Applied Physics Lab, Johns Hopkins University, Silver Spring, Md.

[2] Bannink, W. J. and Nebbeling, C., "Determination of the Position of a Shock Wave from Pitot Tube Experiments," *AIAA Journal*, Vol. 7, No. 4, April 1969, pp. 796–797.

A Quantitative Measurement of Thermally Induced Stress Waves

C. M. Percival*
Sandia Laboratories, Albuquerque, N. Mex.

SINCE the paper by Danilovskaya[1] in 1950 many authors have considered the theory of the dynamic behavior of elastic materials upon exposure to very rapid heating such as can occur on exposure to electromagnetic radiation of various kinds. When the energy deposition time is of the same order as the mechanical response time of the material, dynamic stresses can develop. These stresses are a result of the material's inertial resistance to rapid thermal expansion. This author, in a previous paper,[2] addressed the problem of thermally generated stress waves in a one-dimensional stress field, the finite rod problem. This paper reported the first measurements of elastic stress waves generated in a solid bar due to in-depth absorption of laser radiation. Papers by Morland[3] and Bushnell and McCloskey[4] dealt with the similar problem in one-dimensional strain. Although the theory presented in these papers is valid, measurements of thermally generated stress waves in good quantitative agreement with the one-dimensional strain theory have not as yet been reported.

This Note will describe such a quantitative measurement of laser generated stress waves in which both the wave shape and amplitude agree with the theoretical predictions. The deposition time and the energy penetration depth in the material are such that the effect of a finite deposition time must be considered.

Experiment

The energy source used in the experiment was a Q-switched ruby laser. The maximum output of the laser was 8 joules in

Received October 26, 1970.
Work supported by U.S. Atomic Energy Commission.
* Staff Member, Composites Research and Development Department.

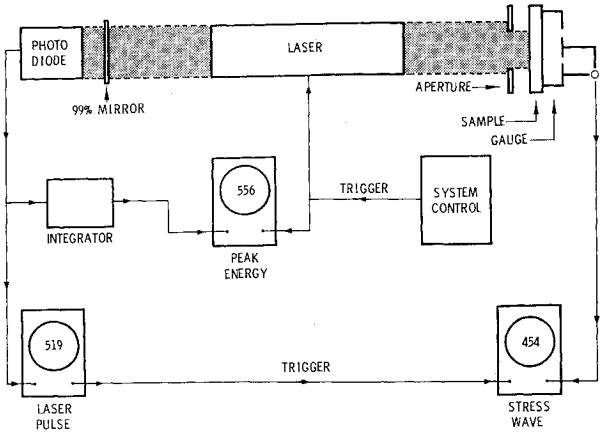

Fig. 1 Schematic of experimental arrangement.

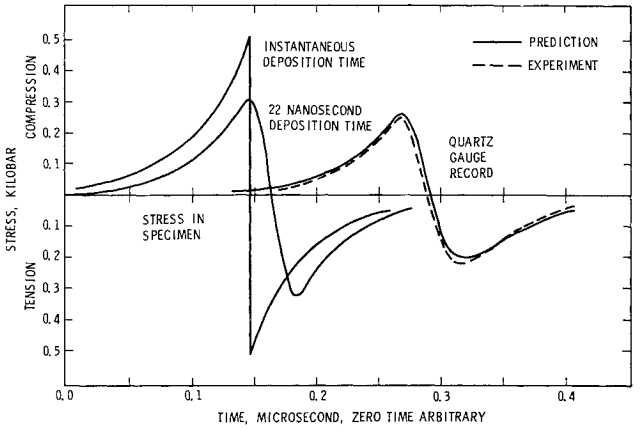

Fig. 3 Stress history.

a pulse having a shape very nearly like the normal distribution with a 22 nanosecond pulse width at half power. The luminous energy was deposited on a piece of Schott BG-18 filter glass, normally used in safety glasses at laser installations. The absorption of the energy by the glass was assumed to be exponential. The skin depth, the depth at which the energy density is $1/e$ (0.369) times that at the front surface, was determined using measurements made on a spectrophotometer and found to be 0.025 cm.

The experimental arrangement is shown in Fig. 1. The output of the laser is determined by monitoring the energy passing through the rear mirror of the optical cavity. The direct output of the monitoring photo diode gives the pulse shape and the integrated diode output is proportional to the total energy. By replacing the specimen with a calorimeter the amount of energy passing through the aperture could be related to the direct and integrated photodiode output. The energy actually impinging on the specimen could thus be measured. Measurements of transmission losses in clear glass show a 10% loss in total transmission. Thus 5% of the energy striking the specimen was assumed reflected at the front surface and the other 95% was absorbed.

A quartz pressure gauge was bonded to the 0.203 cm thick specimen using a polymethyl methacrylate (PMMA) resin and the thickness of the bond was determined to be 0.002 cm. The quartz gauge was 0.635 cm thick and was used in the shorted guard ring configuration[5] with an active area 1.27 cm in diameter. A 1 m piece of RG58 coaxial cable was used to connect the gauge to the Tektronix 454 oscilloscope. The exposed area had a diameter of 1.90 cm which is sufficient to insure a one-dimensional strain configuration. Fig. 2 shows a photographic-oscilloscope record. The electrical rise time of the transducer circuit is approximately 5 nanoseconds, thus the signal should be undistorted during the 50 nanosecond initial rise to peak compressive stress. Attenuation may occur during the sharp discontinuity slightly reducing the peak tensile stress. However, this excursion occurs in 25 nanoseconds which is 5 times the electrical time constant and any attenuation will be slight.

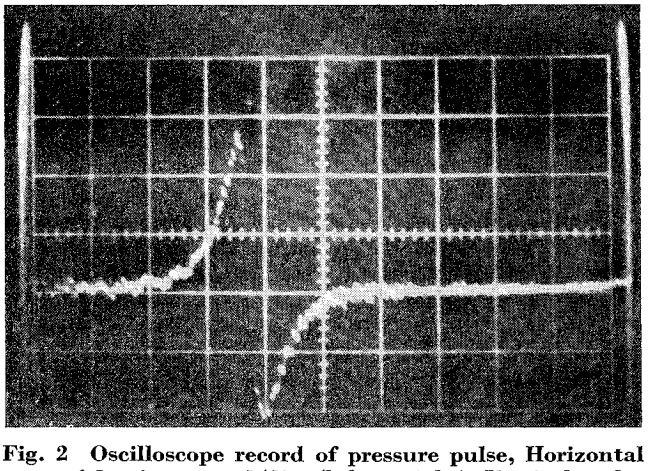

Fig. 2 Oscilloscope record of pressure pulse, Horizontal sweep-0.1 microsecond/div. (left to right), Vertical scale-0.05 volt/div.

Predicted Response

The uniaxial strain response of an absorbing elastic material to a time dependent energy deposition has been predicted using the uncoupled theory of linear thermoelasticity by many authors including Morland[3] and Bushnell and McCloskey.[4] Zaker[6] and Nunziato[7] have considered the same problem using the coupled theory of linear thermoelasticity. The response of an absorbing material can also be predicted using finite difference codes, such as WONDY III[8] which was developed at Sandia Laboratories. Nunziato[7] in the presentation of his work compared the results of all three types of analysis. The comparison between the coupled theory and the finite difference approach was very good with only slight rounding at sharp discontinuities in the traveling wave due to the artificial viscosity used in the finite differencing technique. The uncoupled theory gave a traveling wave with the same amplitude and shape as the coupled theory but displaced slightly in time.

The prediction of the measured response involved two major considerations; they were the effect of the deposition time history and the effect of the acoustic impedance mismatch due to the finite bond thickness and the quartz gauge. An analytical treatment of the propagation of a structured stress wave through layered materials with thickness small compared to the wavelength is difficult; it was decided to solve the whole problem using the finite difference code WONDY III.

The time history of energy deposition was modeled as a symmetric triangular pulse having the same area (total energy) and amplitude (peak power) as a normal distribution with a 22 nanosecond pulse width at half power. Calculations using slightly different time histories with the same total energy indicated that the response was not very sensitive to the pulse shape and the above assumption should be very good.

The elastic constants governing the wave propagation problem are the density, the longitudinal sound speed, and the Grueneisen parameter. BG-18 has a density 2.71 g/cm^3 and a longitudinal sound speed of 0.575 cm/μsec. The density and longitudinal sound speed of PMMA are 1.18 g/cm^3 and 0.275 cm/μsec and for quartz the density is 2.65 g/cm^3 and the longitudinal sound speed 0.572 cm/μsec. The material properties necessary to calculate the Grueneisen parameter of BG-18 glass were measured. They were bulk modulus, 4.49 $\times$ 10^{11} dyne/cm^2; heat capacity, 0.17 cal/

gm°C and linear coefficient of thermal expansion 7.2×10^{-6} cm/cm °C. The resulting Grueneisen parameter is 0.50. WONDY III calculations were made using the above material constants and the experimental geometry; these results are shown in Fig. 3. The stress history for the completely developed wave in the absorbing specimen and the stress history at the front of the quartz gauge are both shown as well as the simple elastic response for instantaneous energy deposition. All theoretical response was calculated to give a peak propagating stress for instantaneous deposition 0.5 kilobar.

Discussion

Figure 3 shows the good agreement between the predicted and measured quartz response. The effect of the finite deposition time is very evident with the reduction and rounding of peak stresses and the increase in the time over which the stress reversal occurs. The effect of impedance mismatch is to reduce the peak stresses and further extend the time for stress reversal.

The experimental record plotted in Fig. 3 is that shown in Fig. 2 scaled to be equivalent to an instantaneous deposition stress of 0.5 kilobar. The actual peak stress for this shot was 0.116 kilobar, for 6.55 joules deposited over the 1.90 cm diameter spot. The measured stress was found to be linear with total deposited energy. If the fluence, joules/unit area, were reduced by a factor of 10, the experimental response was still within 10% of the predicted response. Shots taken at the same fluence level and during the same setup were identical with slight variations, less than 5%, in the stress levels. Similar variations were evident in the energy measurements. At no time did the experimental record vary more than 15% from the predicted response.

It is felt that the three major sources of error in the investigation were in the determination of deposited energy, the pressure measurements and the proper consideration of the effect of the bond thickness. The energy determination was probably made to within ±5%. The pressure measurements, including the errors in reading the traces had less than 10% error. Variations in the bond thickness should not have changed the results by more than 7%. The total experimental error should not have exceeded 20%.

The results of this study show that measurements of thermally generated elastic waves can be made which agree with the theories to well within the normal experimental error. It is questionable that the experimental error can be significantly reduced using the current techniques.

References

[1] Danilovskaya, V. I., "Thermal Stresses in an Elastic Half-Space Arising After a Sudden Heating of Its Boundary," *Prikladnaya Matematika i Mekhanika*, Vol. 14, 1950, pp. 316–318.

[2] Percival, C. M., "Laser-Generated Stress Waves in a Dispersive Elastic Rod," *Journal of Applied Physics*, Vol. 38, 1966, pp. 5313–5315.

[3] Morland, L. W., "Generation of Thermoelastic Stress Waves by Impulsive Electromagnetic Radiation," *AIAA Journal*, Vol. 6, No. 6, June 1968, pp. 1063–1066.

[4] Bushnell, J. C. and McCloskey, D. J., "Thermoelastic Stress Production in Solids," *Journal of Applied Physics*, Vol. 39, 1968, pp. 5541–5546.

[5] Jones, G. A. and Halpin, W. J., "Shorted Guard Ring Quartz Gauge," *Review of Scientific Instruments*, Vol. 39, 1968, pp. 258–259.

[6] Zaker, T. A., "Stress Waves Generated by Heat Addition in an Elastic Solid," *Journal of Applied Mechanics*, Vol. 32, 1965, pp. 143–150.

[7] Nunziato, J. W., "*Radiation Generated Wave Propagation in Elastic Nonconductors*," SC-RR-70-428, June 1970, Sandia Lab., Albequerque, N. Mex.

[8] Lawrence, R. J., "WONDY IIIa—*A Computer Program for One-Dimensional Wave Propagation*," SC-DR-70-315, Aug. 1970, Sandia Laboratories, Albequerque, N. Mex.

Reduced-Order Modeling in Aircraft Mission Analysis

HENRY J. KELLEY*

Analytical Mechanics Associates, Inc., Jericho, N. Y.

A PARTICLE-dynamics model comprising three velocity and three position components is often used for aircraft motion; however, even simpler models are sometimes of value, e.g., the "energy state" model in which vertical motions are presumed executed instantaneously.[1,2] For some purposes, even lower order models as, for example, constant speed are of interest.[3,4] These models are of order six, four, and three, respectively, exclusive of integrations of variable mass. The present note derives an alternate third-order model featuring instantaneously variable speed by means of time-scale separation, further pursuing the approach taken in Refs. 1 and 2.

Energy State Model

The equations of state in energy approximation are, from Ref. 2:

$$\epsilon \dot{E} = V(T - D)/W \tag{1}$$

$$\dot{\chi} = gL \sin\mu / VW \tag{2}$$

$$\dot{x} = V \sin\chi \tag{3}$$

$$\dot{y} = V \cos\chi \tag{4}$$

The state variables are specific energy, $E = h + V^2/2g$, heading angle χ, and rectangular coordinates in the horizontal plane, x and y. The symbol V (velocity) is to be regarded as merely shorthand for $V = [2g(E - h)]^{1/2}$. Control variables are altitude h, bank angle μ, and a throttle variable η appearing in engine thrust T and in aerodynamic drag D (to account for speedbrake control). Drag is evaluated for level turning flight, $L \cos\mu = W$, i.e., this determines angle of attack. Weight W is taken constant for present purposes.

Instantaneously Variable Speed Model

The parameter ϵ appearing on the left of Eq. (1) is unity in the energy state approximation; it is introduced here preparatory to further reduction in order. The Tihonov time-scale separation technique, consisting of progressive reductions in order, was reviewed and applied to aircraft flight in Ref. 2. In that development, heading changes and energy changes were presumed to take place on the same time scale in the second of three groupings. Here, as a gross approximation, energy changes will be idealized as fast compared to heading changes. One sets $\epsilon = 0$, obtaining a reduced-order model, and solves the path-optimization problem (or whatever problem) with the end conditions involving energy E deleted, then accounts for energy transition to specified initial and terminal values in boundary-layer approximation, i.e., by local corrections calculated as afterthoughts. Boundary-layer corrections in optimization problems are dealt with in Refs. 2 and 5. Attention will focus in the following on the "reduced system" obtained from Eqs. (1–4) for $\epsilon = 0$.

With vanishing ϵ, the condition $V(T - D) = 0$ represents a constraint on the four control variables h, μ, η, E. Note that the variable E, and hence speed V, can now jump! For aircraft whose maximum level flight speeds are determined by available power and not by Mach number flight placard, two

Received August 21, 1970; revision received October 23, 1970.

* Vice President. Associate Fellow AIAA.